Supporting Information

Multifunctional SEI-like structure coating stabilizing Zn anode at large current and capacity

Aosai Chen, [a] Chenyang Zhao, [a] Zhikun Guo, [a] Xingyuan Lu, [a] Jiachi Zhang, [a] Zeping Liu, [a] Ming Wang, [a] Nannan Liu, [a] Lishuang Fan, [a,b] Yu Zhang,[*,c] and Naiqing Zhang[*,a,b]

Experimental Procedures

1. Chemicals:
3,4-Dimethoxy-3-cyclobutene-1,2-dione, aniline, zinc trifluoromethylsulfonate, tris(aminoethyl)amine, ammonium molybdate $(NH_4)_6Mo_7O_{24}$, zinc acetate $Zn(CH_3COO)_2$, manganese sulfate ($MnSO_4$), ammonium sulfate ($(NH4)_2SO_4$), ammonium persulfate ($(NH_4)_2S_2O_8$), urea and polyvinyl alcohol (PVA) were purchased from Aladdin. Zinc foils (100μm and 50μm) were purchased from Sinopharm. 50μm zinc foils were used for SEM section and 100μm zinc foils were used for the rest.
2. Materials preparation:
Nano $ZnMoO_4$: Dissolve 0.2g $(NH_4)_6Mo_7O_{24}$ and 1mmol $Zn(CH_3COO)_2$ in 10mL ultrapure water, then add 0.24g urea. The mixed solution was hydrothermally reacted at 150°C for 10 hours. After naturally cooled to room temperature, it was filtered, washed with water, and dried at 60°C for 4 hours.
SR: 2g dimethyl squarate (14.07mmol, 1equir) was dissolved in 20mL anhydrous methanol, then reacted with 1.5g aniline (16.11mmol, 1.15equir) under stirring at room temperature for 24 h. The intermediate product was obtained after filtration and washing with anhydrous methanol. Then 325mg intermediate added to 20mL anhydrous ethanol containing 25mg $Zn(OTf)_2$, followed by 50mg tris(aminoethyl)amine and stirred at room temperature for 24h, the final product was then filtered and washed with anhydrous ethanol, drying in oven at 60℃ for 24h.
PVA gel: Weigh 1g PVA and add into 7mL deionized water, stirring in a water bath at 95°C until dissolved completely. After vacuum defoaming for 4h, it was frozen at -15°C and taken out to thaw at room temperature. Cycling this freeze-thaw operation three times to obtain a PVA gel. PVA@SR is obtained by adding SR before vacuum defoaming and performing subsequent operations.
α-MnO_2: Dissolving 0.2M $MnSO_4$, 0.2M $(NH_4)_2S_2O_8$, 0.8M $(NH4)_2SO_4$ to get 40mL aqueous solution, then transferred into 50mL PTFE lining and sealed in stainless steel autoclave, heat treated at 140℃ for 12h.
3. Electrode preparation:
Modified Zn: nano-$ZnMoO_4$ powder and appropriate amount of NMP were mixed and stirred for 12h to obtain casting slurry. The obtained slurry was cast onto the zinc foil and then dried in an oven at 60°C for 12h to remove the solvent. Then PVA@SR precursor slurry is applied and its fluidity is used to completely fill the empty voids between the particles of $ZnMoO_4$. The hybrid inner layer was obtained after a three freeze-thaw cycles. Then continue to coat the PVA@SR precursor slurry on the hybrid inner layer and perform rapid freeze-thaw cycles to obtain the final SEI-like structure coating modified Zn anode.

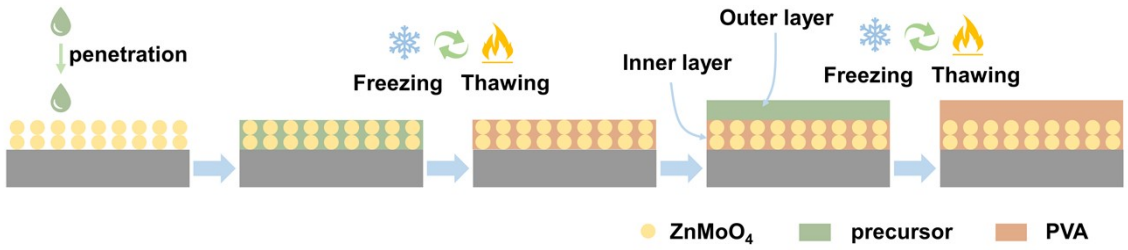

Scheme S1. Detailed preparation of SEI-like structure modified Zn anode.

The cathode material consisted of active material 70wt% α-MnO_2 powder, 20wt% super-P conductor and 10wt% PVDF binder (pre-dissolved in NMP), mixed with appropriate amount of NMP to make a paste and then coated on carbon paper by a simple blade coating strategy. The button cell was assembled in air environment from positive electrode, zinc negative electrode and glass fiber separator, where the glass fiber was between the positive and negative electrodes and impregnated with 100μL of 3M $ZnSO_4$ + 0.1M $MnSO_4$ aqueous electrolyte.
4. Electrochemical characterizations:
Hydrogen evolution test and cyclic voltammetry (CV) were carried on an electrochemical workstation (Chenhua Shanghai). Tafel and chronoamperometry (CA) measurements were conducted in three-electrode configuration, in which bare Zn and modified Zn foils were used as the working electrode, Pt plate as the counter, and Ag/AgCl electrode as the reference. EIS spectra were recorded on the PAR2273 electrochemical workstation with a frequency range from 1 MHz to 0.01 Hz.
5. Electrochemical Measurement:
The specification of our battery is 2032 button cell, the diameter of the zinc disc anode is 12 mm and the thickness is 50 μm. The cathode carrier is carbon paper with a diameter of 10 mm, and the active material loading is around 1.5 mg cm^{-2}. The separator is Whatman fiber separator. The electrolyte for the symmetric cell is 3.0 M $ZnSO_4$ aqueous solution, and the electrolyte for the full cell is 3.0 M $ZnSO_4$ + 0.5 M $MnSO_4$ aqueous solution. The current densities and specific capacities of full cell cycling were determined based on the mass of cathode active material.
6. Material characterizations:
Surface morphology of materials were characterized by scanning electron microscopy (SEM; Hitachi, SU8010), equipped energy dispersive x-ray spectroscopy (EDS) for the elemental composition and distribution. X-ray diffraction (XRD, PANalytical X'Pert PRO, Cu Kα radiation) recorded the diffraction patterns of materials. The Raman spectra were performed by Renishaw inVia microscope

with a wavelength and resolution of 532 nm and 2 cm^{-1}, respectively. The zinc deposition behavior and hydrogen evolution situation were monitored by in- situ optical microscopy in real time.

7. DFT calculation:

Density functional theory calculations were carried out by the Vienna Ab-initio Simulation Package (VASP) with the projector augmented wave (PAW) method. The generalized gradient approximation (GGA) with the Perdew-Burke-Ernzerhof (PBE) was adopted to describe the exchange. Furthermore, the DFT-D3 method was adopted to describe the van der Waals corrections. The cutoff energy was set to 400 eV throughout the computations. Partial occupancies of the Kohn−Sham orbitals were allowed under the occasion which uses the Gaussian smearing method and a width of 0.05 eV. These settings ensure convergence of the total energies to within 10^{-5} eV. Structure relaxation proceeded until all forces on atoms were less than 0.03 eV $Å^{-1}$. A Monkhorst-Pack 3 × 3 × 1 k-point mesh was used for energy convergence. The adsorption energy (E_{ads}) was calculated as

$E_{ads} = E_{total} - E_{sub} - E_{Zn}$

E_{total}, E_{sub} and E_{Zn} represent the total energy of TiO_2 substrate combined with zinc atom, the energy of the TiO_2 substrate and the energy of zinc atom, respectively.

Results and Discussion

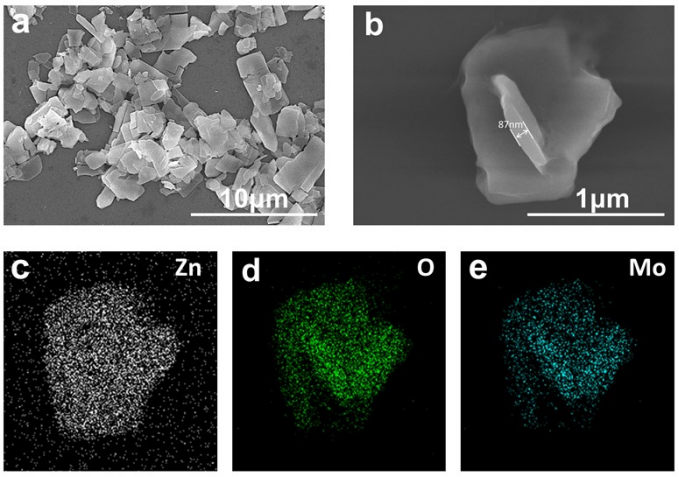

Figure S1. SEM images of nano-$ZnMoO_4$ and related EDS-mapping.

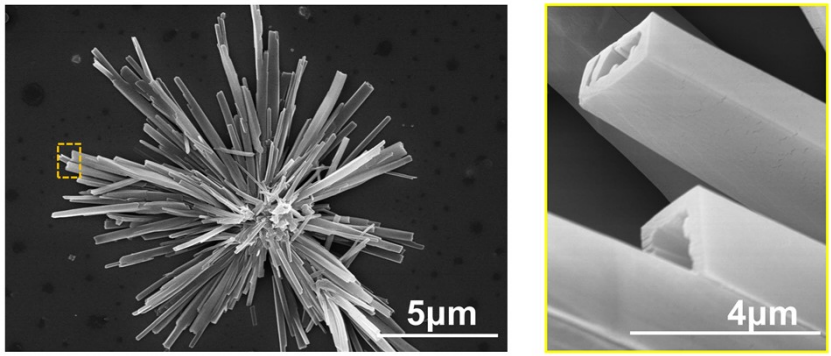

Figure S2. SEM images of SR.

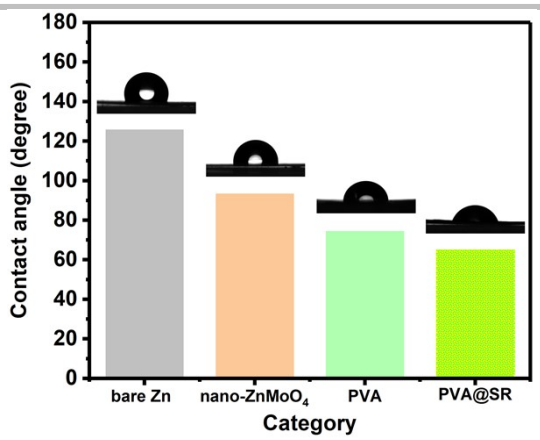

Figure S3. Contact angle of pure PVA gel and modified PVA gel with different SR addition.

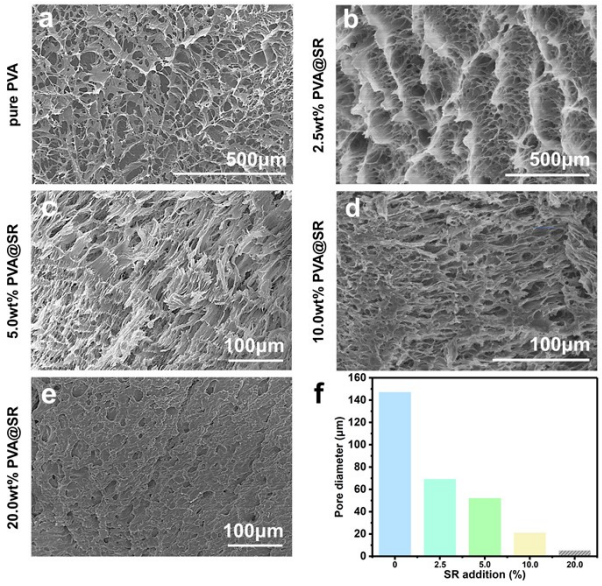

Figure S4. SEM images of PVA gel with different SR addition.

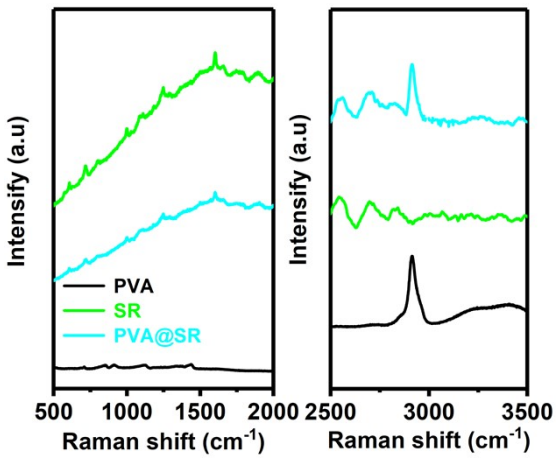

Figure S5. Raman spectra of SR, pure PVA gel and SR modified PVA gel.

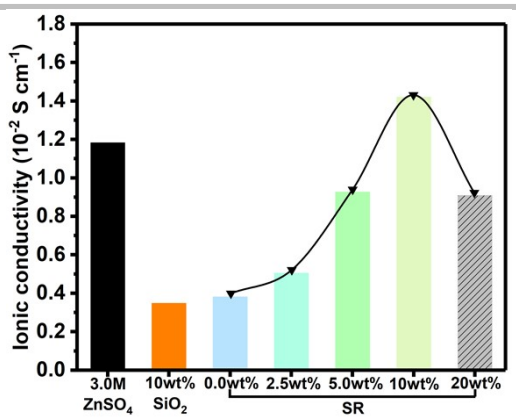

Figure S6. Ionic conductivity of 3.0M $ZnSO_4$ electrolyte, 10wt% PVA@SiO_2 and modified PVA gels with different SR addition.

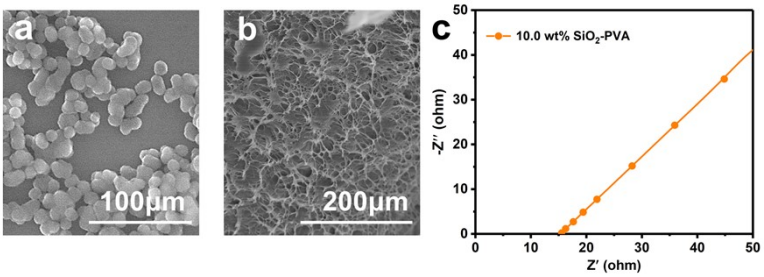

Figure S7. SEM images of nano-SiO_2 (a) and 10wt% SiO_2 modified PVA (b), relative EIS spectrum.

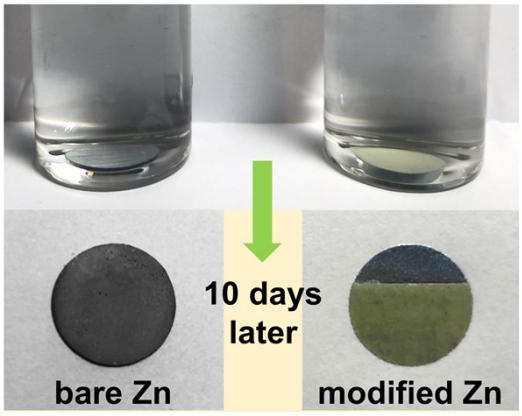

Figure S8. Passivation resistance and coating stability of modified Zn anode.

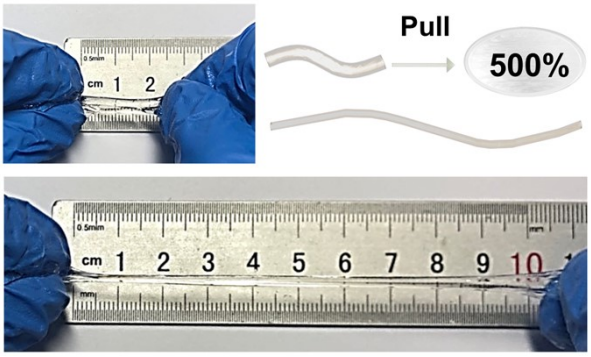

Figure S9. Ductility of pure PVA gel.

Figure S10. Optical images of modified Zn foil at twisting, bending states and corresponding flat states.

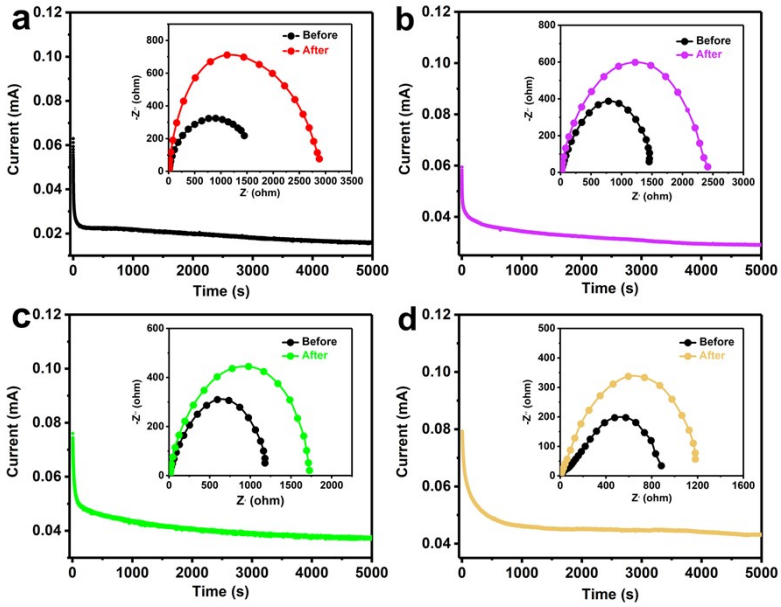

Figure S11. Zn^{2+} transference number for (a) bare Zn, (b) $ZnMoO_4$ coated Zn, (c) SR coated Zn and SEI-like coating modified Zn after polarization at a constant potential (10 mV) for 5000 s. The insets are the impedance spectra before and after polarization.

For transfer number testing, symmetric cells with bare Zn, $ZnMoO_4$ modified Zn, PVA@SR modified Zn and SEI-like coating modified Zn were assembled separately, and the electrolyte was 3.0 M $ZnSO_4$ aqueous solution. The time-current curves of the cells at a polarization voltage of 10 mV and the EIS spectra before and after polarization were tested. The transfer number of the cell was calculated using the following equation:

$$t_{Zn^{2+}} = \frac{I_s(\Delta V - I_0 R_0)}{I_0(\Delta V - I_s R_s)}$$

where ΔV is the constant polarization voltage applied (10 mV here), I_0 and R_0 are the initial current and resistance, and I_s and R_s are the steady-state current and resistance, respectively.

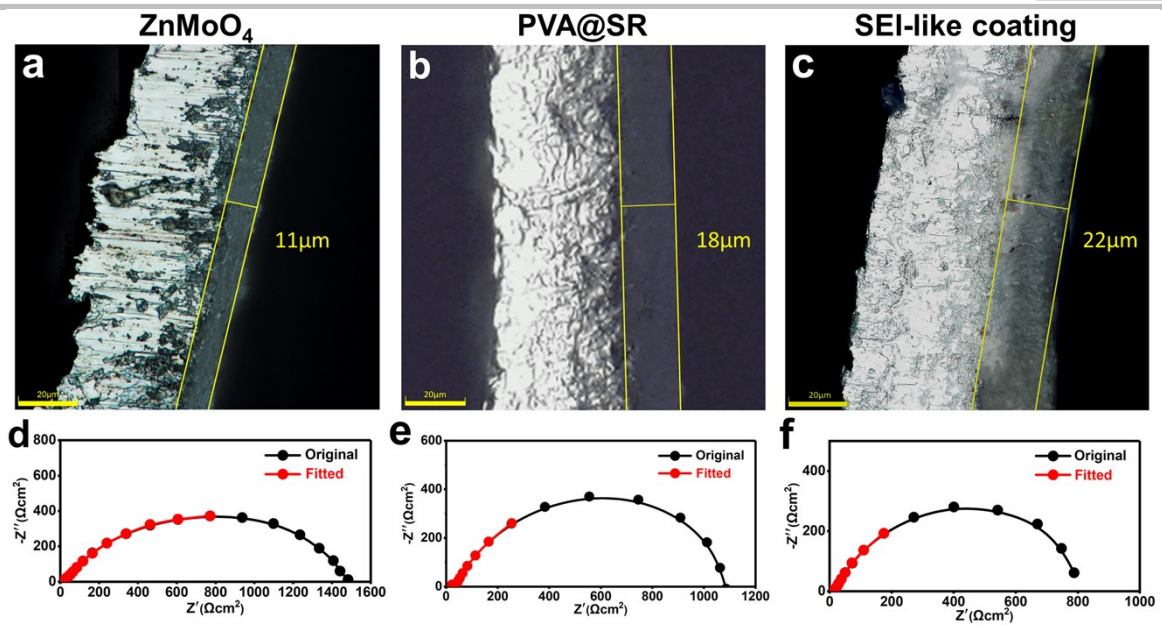

Figure S12. Confocal Laser Scanning Microscope (CLSM) images (a-c) and EIS fitting spectra (d-f).

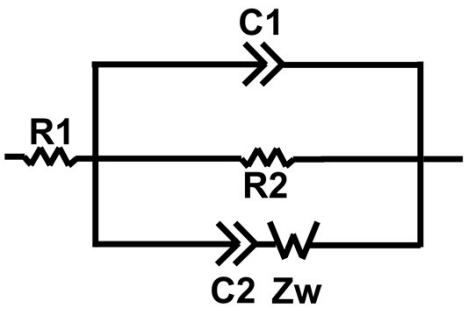

Figure S13. The equivalent circuit for the EIS fit.

The ionic diffusion coefficient (D_{Zn-ion}) of the modified layer can be calculated by the following equation[1, 2]:

$$Z_w = \frac{D_{Zn-ion}^{1/2} R}{l}$$

Where l is the thickness of the modified layer, R is interfacial impedance, and Z_w is the Warburg element. The thickness of $ZnMoO_4$ coating, PVA@SR coating and SEI-like coating can be measured by Confocal Laser Scanning Microscope (CLSM). The symmetric cells were assembled to test EIS spectra, and the EIS spectra were fitted using EC-Lab (the equivalent circuit is shown in Figure S13). In order to pursue data accuracy, data points with frequency below 20Hz were excluded from the fitting range. Substituting R as well as Z_w obtained from the fitting results into the above equation to obtain D_{Zn-ion}.

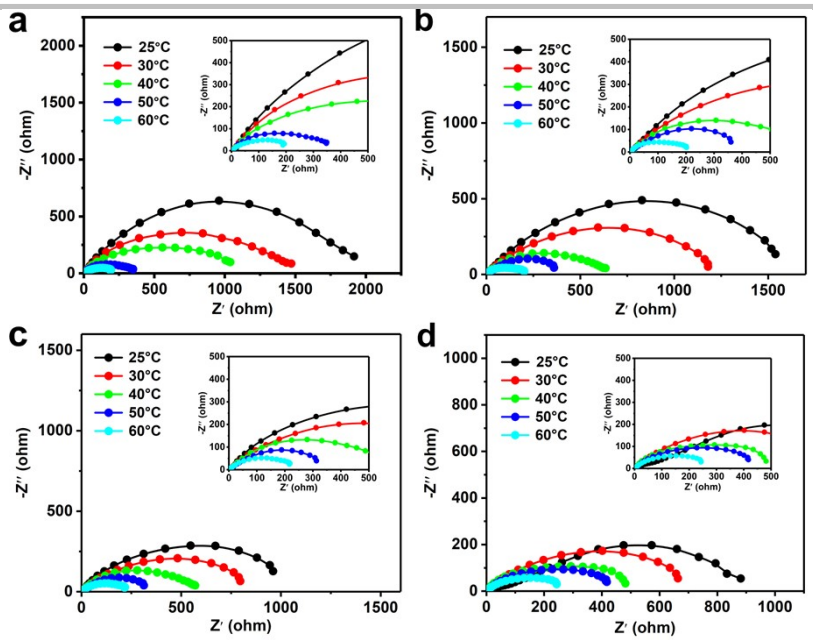

Figure S14. EIS spectra at different temperatures: (a) bare Zn, (b) $ZnMoO_4$ coated Zn, (c) PVA@SR coated Zn, (d) SEI-like coating modified Zn.

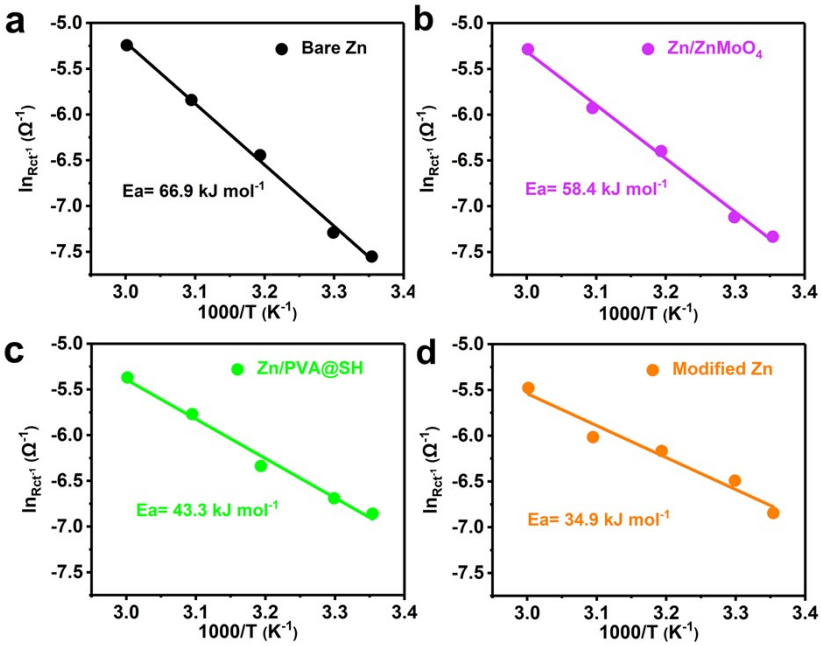

Figure S15. Corresponding activation energy.

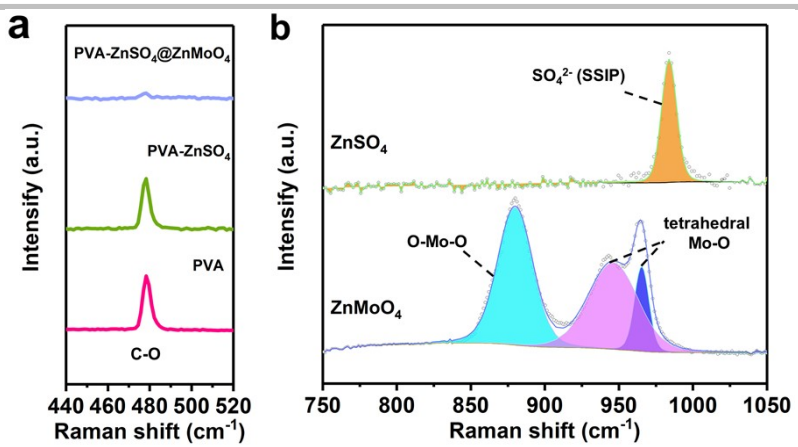

Figure S16. Raman spectra.

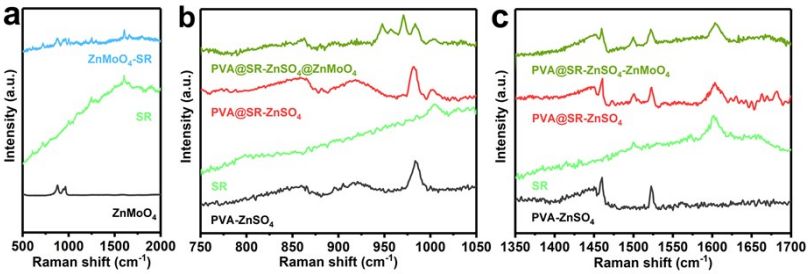

Figure S17. Investigating for compatibility of SR additives. (a) SR to $ZnMoO_4$, (b) and (c) SR to PVA-$ZnSO_4$ and to PVA-$ZnSO_4$@$ZnMoO_4$.

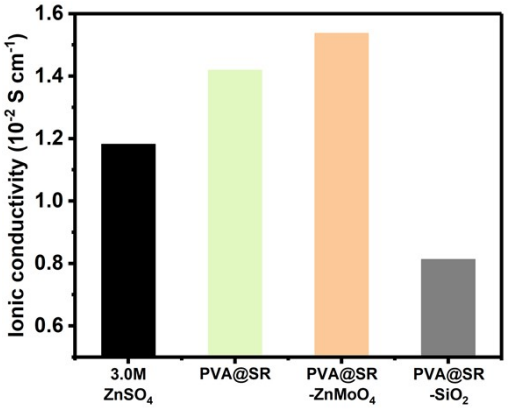

Figure S18. Ionic conductivity comparison of PVA@SR outer layer, PVA@SR-$ZnMoO_4$ coating and PVA@SR-SiO_2 coating.

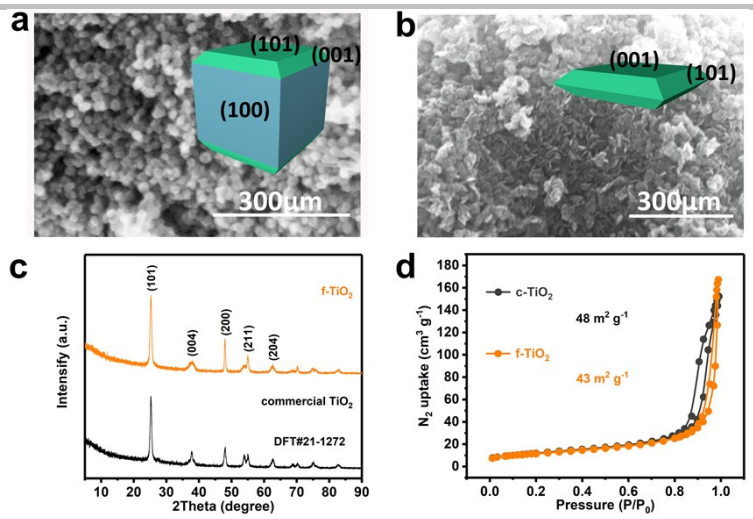

Figure S19. SEM images of (a) c-TiO_2 and f-TiO_2 (b). (c) XRD patterns. (d) Adsorption-desorption curves.

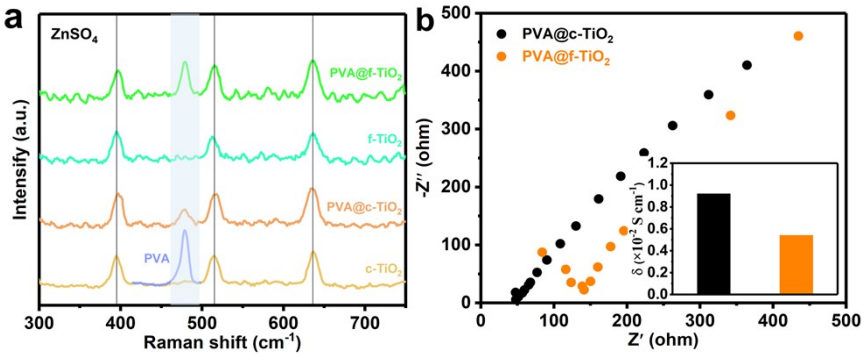

Figure S20. (a) Raman Characterization of synergic effect between TiO_2 and PVA in $ZnSO_4$ system. (b) EIS spectra and corresponding ionic conductivity of Zn^{2+}-PVA@c-TiO_2 and Zn^{2+}-PVA@f-TiO_2.

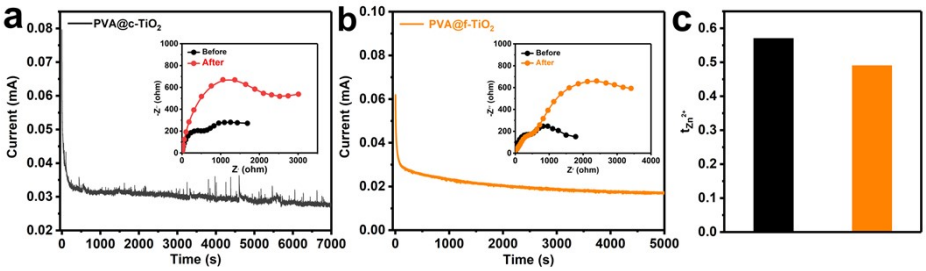

Figure S21. Zn^{2+} transference number for Zn^{2+}-PVA@c-TiO_2 modified Zn and Zn^{2+}-PVA@f-TiO_2 modified Zn.

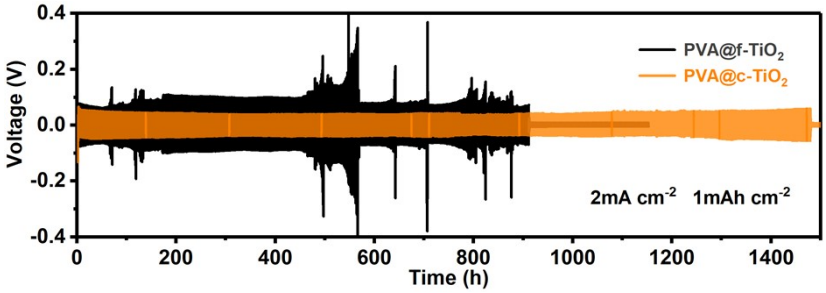

Figure S22. Long-term cycling performance of PVA@f-TiO_2 modified Zn and PVA@c-TiO_2 modified Zn symmetric cells.

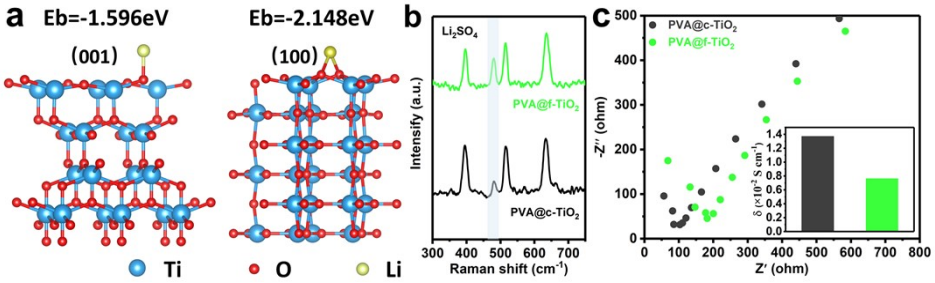

Figure S23. (a) Binding energy of Li^+ on TiO_2 (001) and (100). (b) Raman Characterization of synergic effect between TiO_2 and PVA in Li_2SO_4 system. (c) EIS spectra and corresponding ionic conductivity of Li^+-PVA@c-TiO_2 and Li^+-PVA@f-TiO_2.

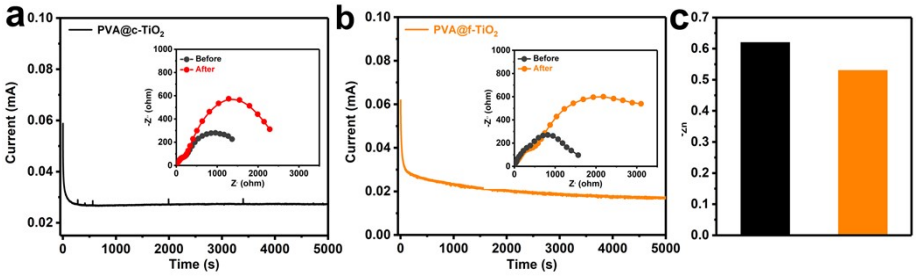

Figure S24. Li^+ transference number for Li^+-PVA@c-TiO_2 modified Zn and Li^+-PVA@f-TiO_2 modified Zn.

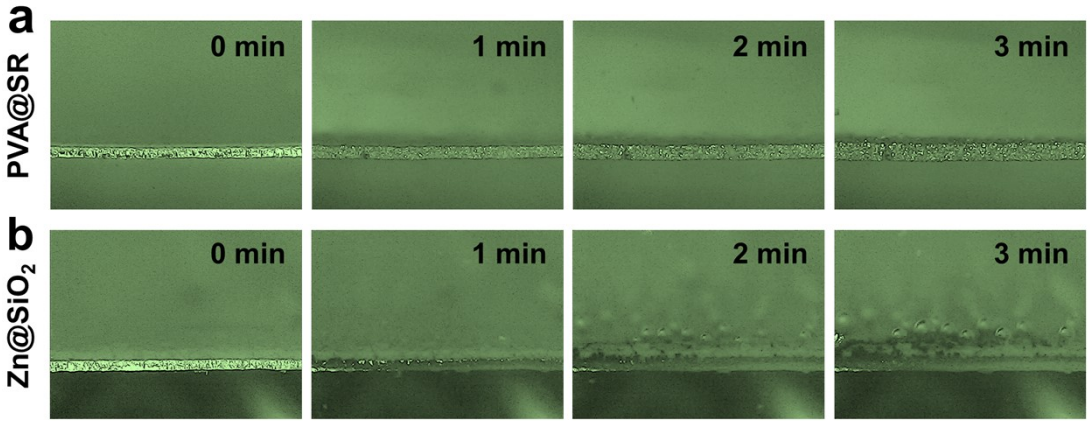

Figure S25. In-situ optical microscopy of PVA@SR (a) coated Zn and PVA@SiO_2 (b) coated Zn. The $ZnMoO_4$ coated Zn can be seen in previous report[3].

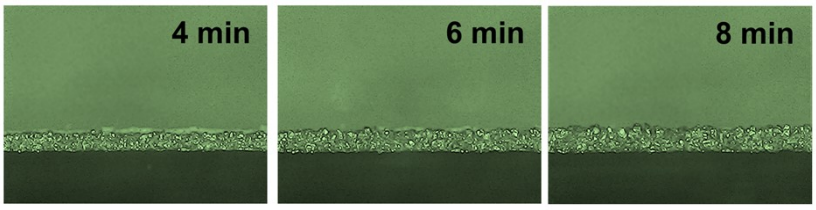

Figure S26. Subsequent in-situ optical microscopy of PVA@SR-$ZnMoO_4$.

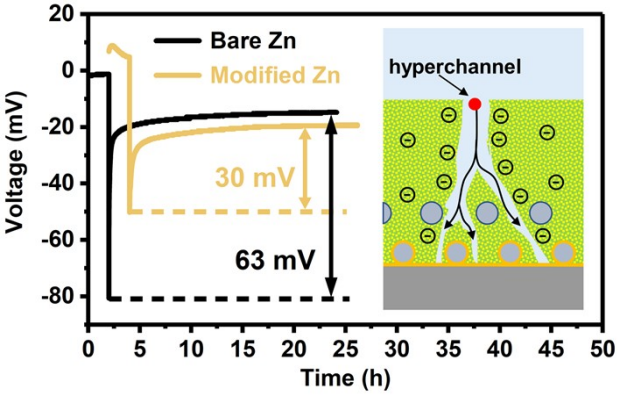

Figure S27. Zinc nucleation overpotential.

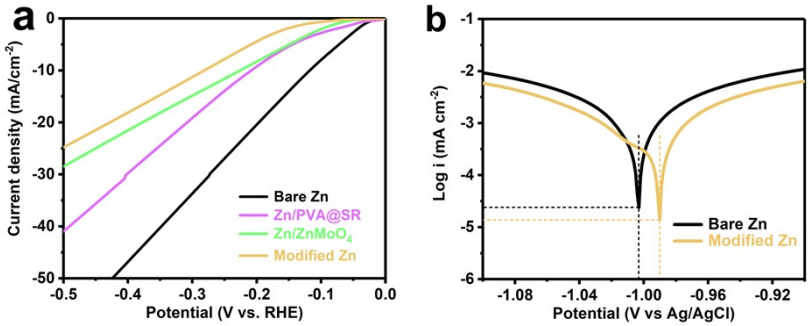

Figure S28. (a) LSV plots. (b) Tafel curves.

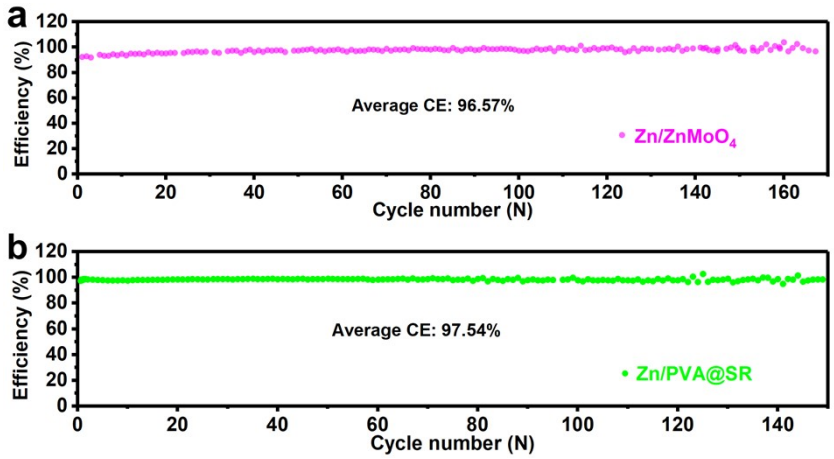

Figure S29. Long-term coulombic efficiency of $ZnMoO_4$ modified Zn and PVA@SR modified Zn at 0.5mA cm^{-2} and 0.5mAh cm^{-2}.

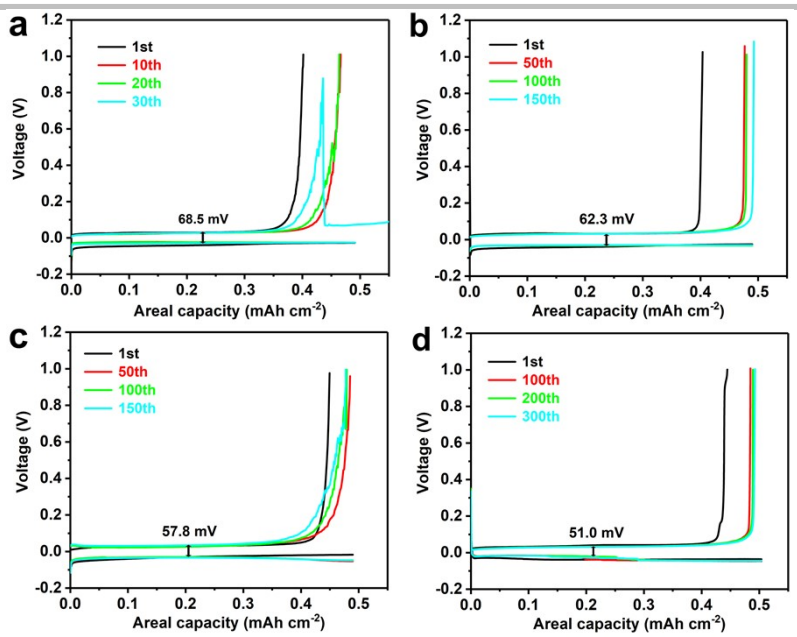

Figure S30. Related capacity-voltage plots of (a) bare Ti, (b) $ZnMoO_4$ coated Ti, (c) PVA@SR coated Ti, (d) SEI-like coating modified Ti.

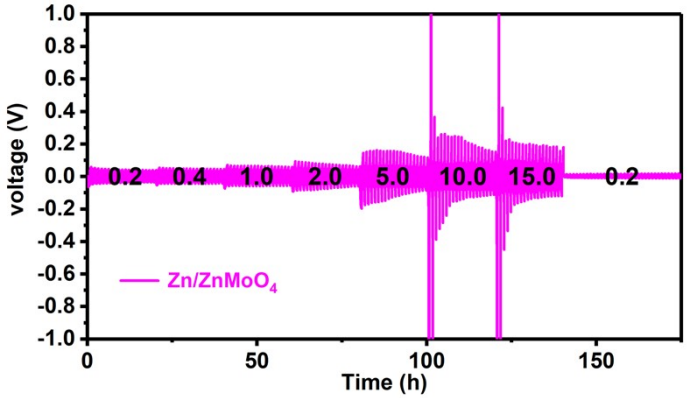

Figure S31. Rate performance of $ZnMoO_4$ coated Zn.

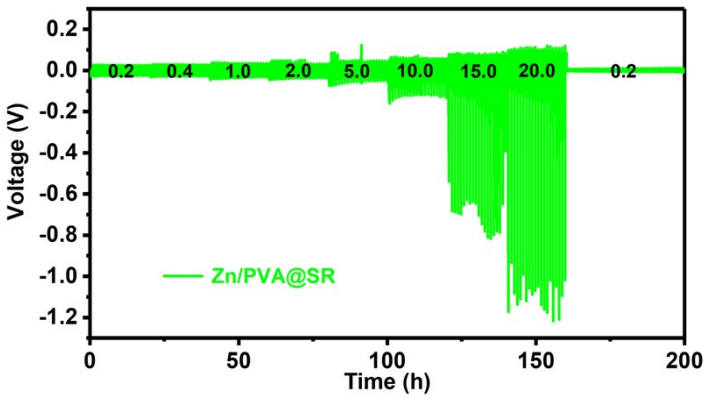

Figure S32. Rate performance of PVA@SR coated Zn.

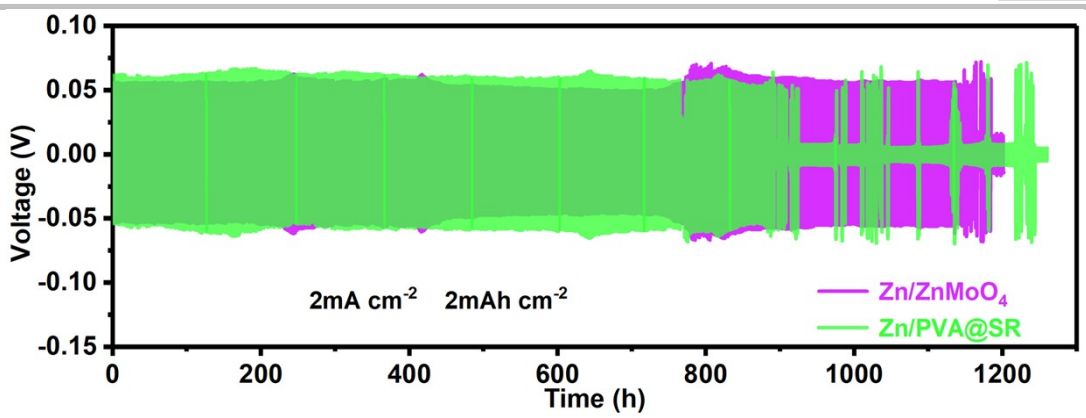

Figure S33. Long-term cycling performance of $ZnMoO_4$ modified Zn and PVA@SR modified Zn symmetric cells.

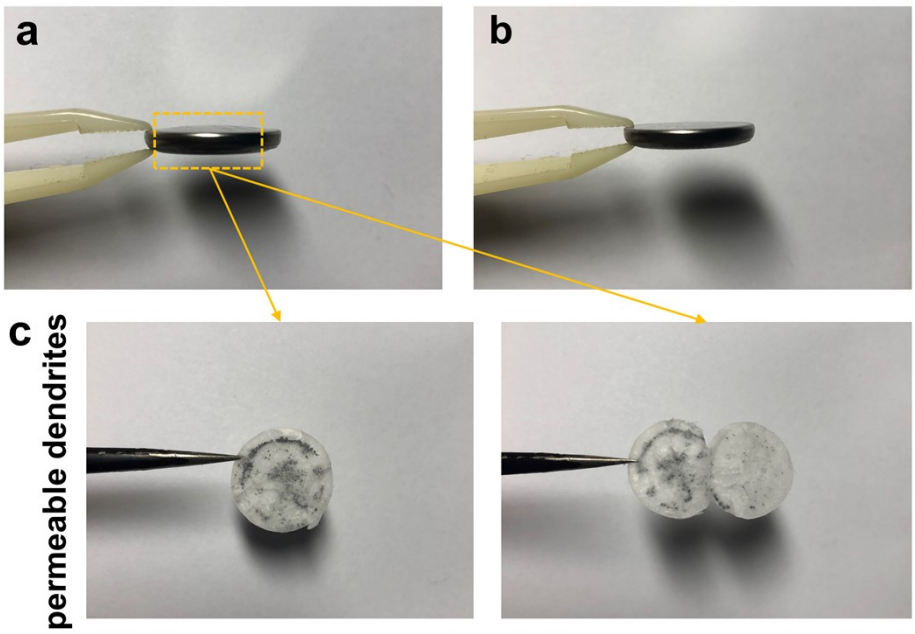

Figure S34. Bulging comparison of bare Zn battery (a) and modified Zn battery (b). Permeable dendrites in bare Zn battery separator.

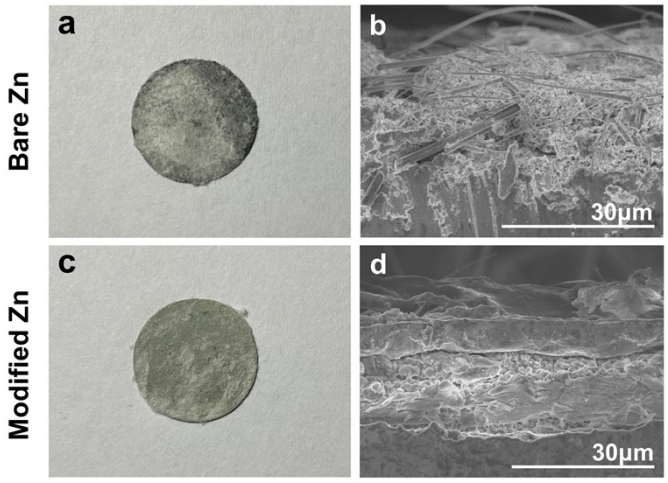

Figure S35. Corresponding optical and SEM images of bare and modified Zn anodes after cycle.

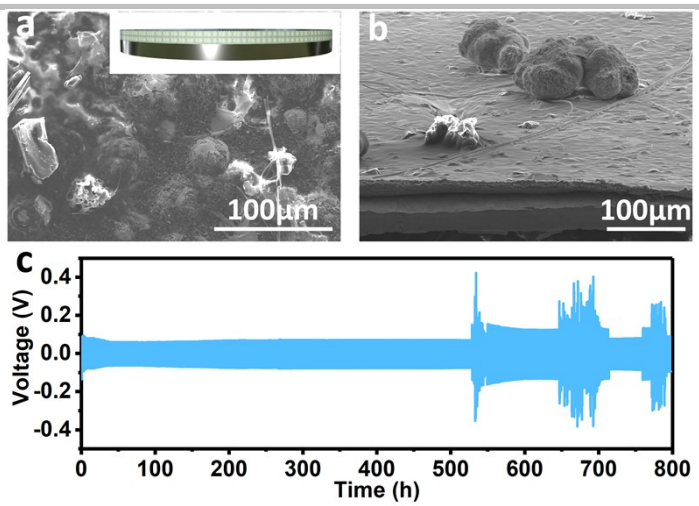

Figure S36. (a) Front and (b) side SEM images of SEI-like coating without overlayer modified Zn with 2mAh cm^{-2} plated zinc. (c) Long-term cycling performance at 5mA cm^{-2} and 5mAh cm^{-2}.

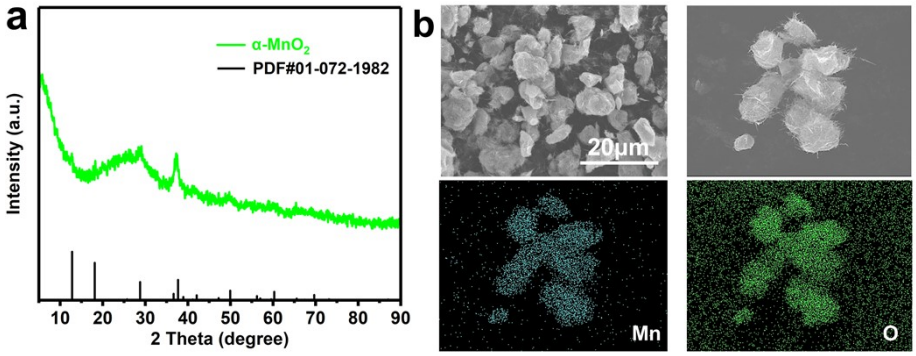

Figure S37. Cathode material α-MnO_2: XRD pattern of (a). SEM image and corresponding EDS-mapping results (b).

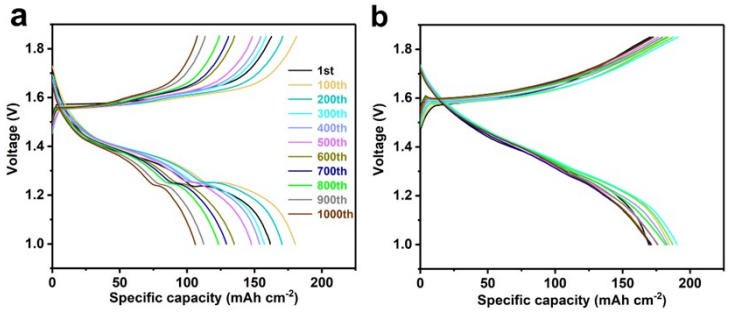

Figure S38. Capacity-voltage curves of the full cells with (a) bare Zn and (b) modified Zn at different cycle numbers.

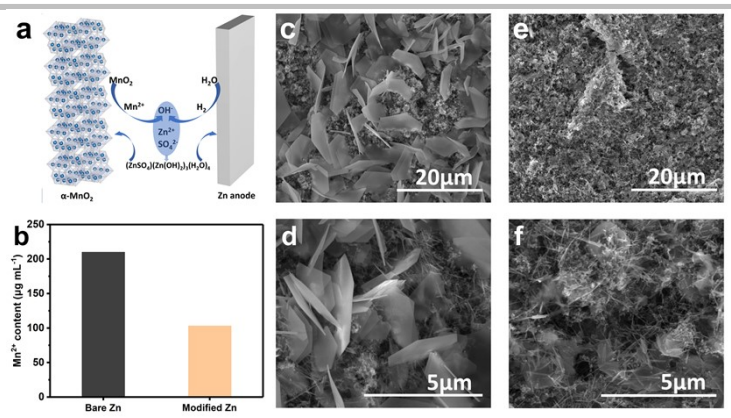

Figure S39. (a) Schematic diagram showing the reactions of α-MnO_2/Zn battery using $ZnSO_4$ aqueous electrolyte during cycling. (b) ICP results of α-MnO_2 dissolution after 20 cycles at 1A g^{-1}. Corresponding SEM images of α-MnO_2 cathode: (c) and (d) bare Zn battery, (e) and (f) modified Zn battery.

The effect of the coating layer on the cathode material can be explained by the effect on the electrolyte. For example, the hydrogen evolution on the anode surface can affect the concentration and pH of the electrolyte (Reaction b), which in turn changes the operating environment of the cathode and promotes the production of $(ZnSO_4)(Zn(OH)_2)_3(H_2O)_4$ on the anode surface (Reaction c). In addition, hydrogen adsorption and $(ZnSO_4)(Zn(OH)_2)_3(H_2O)_4$ coverage on the cathode surface can reduce the active area and promote the disproportionate reaction of MnO_2 dissolution and generate more OH^- (Reaction a), forming a vicious circle.

$$MnO_2 + 2H_2O + 2e^- \rightarrow Mn^{2+} + 4OH^- \quad \text{(Reaction a)}$$

$$2H_2O + 2e^- \rightarrow H_2 + 2OH^- \quad \text{(Reaction b)}$$

$$4Zn^{2+} + SO_4^{2-} + 6OH^- + 4H_2O \rightarrow (ZnSO_4)(Zn(OH)_2)_3(H_2O)_4 \quad \text{(Reaction c)}$$

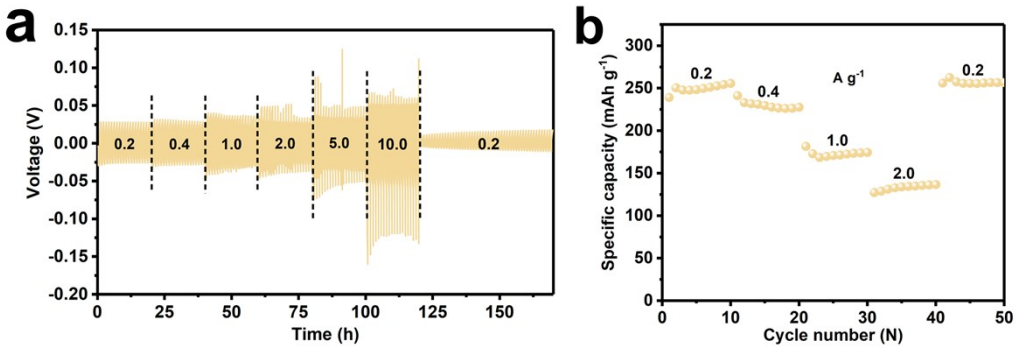

Figure S40. Rate performance of modified Zn symmetric battery(a) and modified Zn/α-MnO_2 full battery(b) without liquid electrolyte.

Table S1. Parameters for the EIS measurements and equivalent circuit fits used to calculate Zn-ion transport properties of the coating.

Coating	l (cm)	R_{SEI} (Ω)	Zw ($Ωs^{-0.5}$)	$D_{Zn\text{-}ion}$ (cm^2/s)
$ZnMoO_4$	$1.1×10^{-3}$	1483	10588	$6.17×10^{-5}$
PVA@SR	$1.8×10^{-3}$	1085	26167	$1.89×10^{-3}$
SEI-like coating	$2.2×10^{-3}$	788	35973	$1.01×10^{-2}$

Table S2. Raman analysis of PVA, $ZnSO_4$ and $ZnMoO_4$.

Category	Raman shifit (cm^{-1})	Polarization	Assignment
PVA	478	bending	C-O
	822	stretching	C-C
	852		
	893	rocking	CH_2
	922		
	1432	bending	CH
	1450	bending	OH
	1462	shear mode	CH_2
	1563	stretching	C-O
$ZnSO_4$	980	stretching	SO_4^{2-} (SSIP)
	993	stretching	SO_4^{2-} (CIP)
$ZnMoO_4$	880	stretching	O-Mo-O
	945	stretching	tetrahedral Mo-O bond
	965		

Table S3. Comparison of typical parameters and cycling performance for this work with recently reported Zn-based symmetric cell.

Coatings	Current density ($mA\ cm^{-2}$)	Areal capacity ($mAh\ cm^{-2}$)	Cycle time (h)	Reference
ZnO-3D	5	1.25	500	EES,2020[4]
$Zn_3(PO_4)_2{\cdot}4H_2O$	1	1	1200	AM,2021[5]
CNG	1	0.5	3000	EES,2021[6]
ZSO	5	1	1500	AM,2022[7]
IS	5	2.5	800	ACS Nano,2022[8]
	5	5	500	
DTPMP	5	0.5	1300	ACS Nano,2022[9]
PFSA	1	1	800	ACS Nano,2022[10]
Nafion-$Zn_3(PO_4)_2$	2	1	900	EnSM,2022[11]
Nafion-Zn-X zeolite	5	0.5	2000	Angew. Chem. 2020[12]
	2	**2**	**2000**	
$ZnMoO_4$-PVA@SR	**5**	**5**	**1700**	**This work**
	10	**10**	**250**	

References

1. R. Guo and B. M. Gallant, *Chem. Mater.*, 2020, **32**, 5525-5533.
2. D. T. Boyle, Y. Li, A. Pei, R. A. Vila, Z. Zhang, P. Sayavong, M. S. Kim, W. Huang, H. Wang, Y. Liu, R. Xu, R. Sinclair, J. Qin, Z. Bao and Y. Cui, *Nano Lett.*, 2022, **22**, 8224-8232.
3. A. Chen, C. Zhao, Z. Guo, X. Lu, N. Liu, Y. Zhang, L. Fan and N. Zhang, *Energy Storage Mater.*, 2022, **44**, 353-359.
4. X. S. Xie, S. Q. Liang, J. W. Gao, S. Guo, J. B. Guo, C. Wang, G. Y. Xu, X. W. Wu, G. Chen and J. Zhou, *Energy Environ. Sci.*, 2020, **13**, 503-510.
5. X. Zeng, J. Mao, J. Hao, J. Liu, S. Liu, Z. Wang, Y. Wang, S. Zhang, T. Zheng, J. Liu, P. Rao and Z. Guo, *Adv. Mater.*, 2021, **33**, e2007416.
6. X. T. Zhang, J. X. Li, D. Y. Liu, M. K. Liu, T. S. Zhou, K. W. Qi, L. Shi, Y. C. Zhu and Y. T. Qian, *Energy Environ. Sci.*, 2021, **14**, 3120-3129.
7. R. Guo, X. Liu, F. Xia, Y. Jiang, H. Zhang, M. Huang, C. Niu, J. Wu, Y. Zhao, X. Wang, C. Han and L. Mai, *Adv. Mater.*, 2022, **n/a**, e2202188.
8. S. Jiao, J. Fu, M. Wu, T. Hua and H. Hu, *ACS Nano*, 2021, **16**, 1013-1024.
9. H. Yu, Y. Chen, W. Wei, X. Ji and L. Chen, *ACS Nano*, 2022, **16**, 9736-9747.
10. L. Hong, X. Wu, L. Y. Wang, M. Zhong, P. Zhang, L. Jiang, W. Huang, Y. Wang, K. X. Wang and J. S. Chen, *ACS Nano*, 2022, **16**, 6906-6915.
11. S. J. Wang, Z. Yang, B. T. Chen, H. Zhou, S. F. Wan, L. Z. Hu, M. Qiu, L. Qie and Y. Yu, *Energy Storage Mater.*, 2022, **47**, 491-499.
12. Y. Cui, Q. Zhao, X. Wu, X. Chen, J. Yang, Y. Wang, R. Qin, S. Ding, Y. Song, J. Wu, K. Yang, Z. Wang, Z. Mei, Z. Song, H. Wu, Z. Jiang, G. Qian, L. Yang and F. Pan, *Angew Chem Int Ed Engl*, 2020, **59**, 16594-16601.